

Construction and Application of a Pollen Emissions Model based on Phenology and Random Forests

3 Jiangtao Li^{a,b}, Xingqin An^{a,*}, Zhaobin Sun^a, Caihua Ye^c, Qing Hou^a, Yuxin Zhao^a, Zhe
4 Liu^a

⁵ ^a State Key Laboratory of Severe Weather, Chinese Academy of Meteorological
⁶ Sciences, Beijing, 100081, China

⁷ ^b Department of Atmospheric and Oceanic Sciences & Institute of Atmospheric
⁸ Sciences, Fudan University, Shanghai, 200438, China

⁹ ^c Meteorological Service Center of Beijing Meteorological Bureau, Beijing, 100089,
¹⁰ China

11 * Corresponding author: Xingqin An

12 Email address: anxq@cma.gov.cn

13 **Abstract:** In recent years, the intensification of global climate change and
14 environmental pollution has led to a marked increase in pollen-induced allergic
15 diseases. This study leverages 16 years of continuous pollen monitoring data,
16 alongside meteorological factors and plant functional type data, to construct a pollen
17 emissions model using phenology and random forests (RF). This model is then
18 employed to simulate the emission characteristics of three primary types of autumn
19 pollen (Artemisia, Chenopod, and total pollen concentration), elucidating the emission
20 patterns throughout the seasonal cycle in Beijing. Phenology and RF precisely
21 simulate the start and end day of year of pollen, as well as the annual pollen
22 production. There are significant spatiotemporal differences among the three types of
23 pollen. On average, pollen dispersal begins around August 10, peaks around August
24 30, and concludes by September 25, with a dispersal period lasting approximately 45
25 days. Furthermore, the relationship between pollen emissions and meteorological
26 factors is investigated, revealing that temperature, relative humidity (RH), and
27 sunshine hours (SSH) significantly influence annual pollen emissions. Specifically,
28 temperature and RH exhibit a strong positive correlation with annual pollen emissions,

29 while SSH shows a negative correlation. Different pollen types display varied
30 responses to meteorological factors. Finally, the constructed pollen emissions model is
31 integrated into **Regional Climate Model (RegCM)** and validated using pollen
32 observation data, confirming its reliability in predicting pollen concentrations. This
33 study not only enhances the understanding of pollen release mechanisms but also
34 provides scientific evidence for the selection and planting of urban greening plants.

35 **Keywords:** Pollen Emissions Model, Phenology, Random Forests, RegCM

36 1. Introduction

37 Pollen are microscopic particles, typically ranging from 5 to 100 micrometers in
38 diameter, released by plants to transfer male genetic material for reproduction. These
39 particles, significant allergens, disperse into the atmosphere via wind, contributing to
40 atmospheric particulate matter, interacting with clouds and radiation, and playing a
41 pivotal role in plant fertilization and gene dissemination (Damialis et al., 2011; Lei et
42 al., 2023). Additionally, pollen is linked to allergic diseases such as allergic rhinitis
43 and asthma and may even elevate the risk of gastrointestinal and neurological
44 disorders (Guzman et al., 2007; Krishna et al., 2020; Chen et al., 2021; Stas et al.,
45 2021). In China, the incidence of pollen allergies has surged from 5 % to 17.8 % and
46 continues to rise rapidly (Lou et al., 2017). Pollen-induced respiratory allergic
47 symptoms, such as allergic rhinitis (AR), affect up to 30 % of the global population,
48 particularly children under 18 (Mir et al., 2012; Wang et al., 2016; Zhang and Steiner,
49 2022; Zhao et al., 2023). It is generally believed that these respiratory allergic
50 diseases are more prevalent in developed countries (Emanuel, 1988; Ibrahim et al.,
51 2021). However, the International Study of Asthma and Allergies in Childhood
52 (ISAAC) global reports indicate that these diseases are equally or even more prevalent
53 in some developing countries compared to developed ones (Asher et al., 2006; Mallol
54 et al., 2013). Children, as a vulnerable population, are particularly susceptible to AR
55 and its complications (Cingi et al., 2017). Without effective early intervention, allergic
56 symptoms in children can persist throughout their lives, imposing a substantial
57 economic burden on families and healthcare systems (Ahmed et al., 2018) and

58 potentially posing a life-threatening risk (Schmidt, 2016). In China, a densely
59 populated developing country, the proportion of pediatric allergic diseases within the
60 spectrum of childhood illnesses is increasing annually, leading to significant
61 economic and health losses due to medical expenses, impacts on human life, and
62 premature death (National Cooperative Group on Childhood Asthma, 1993, 2003,
63 2013). Furthermore, since pollen release is closely linked to environmental factors,
64 climate change may influence pollen release, thereby affecting the incidence of
65 allergic diseases (Wang et al., 2018; Bishan et al., 2020). In recent decades, the pollen
66 season has exhibited a trend of becoming longer and more intense, which may
67 exacerbate the conditions of allergic rhinitis and asthma (D'Amato et al., 2016; Lake
68 et al., 2017a; Aerts et al., 2020; Kurganskiy et al., 2021).

69 With the improvement in living standards and heightened health awareness,
70 airborne pollen diseases, such as hay fever, have garnered widespread attention. As a
71 typical seasonal epidemic (Yin et al., 2005; Lei et al., 2023), hay fever significantly
72 impacts global health. Existing studies have demonstrated that the incidence of
73 airborne pollen diseases is closely associated with the concentration of airborne
74 allergenic pollen, particularly during peak pollen seasons (Frei and Gassner, 2008;
75 Bastl et al., 2018; Kurganskiy et al., 2021). Due to the regional nature of airborne
76 pollen, the types and concentrations of pollen vary geographically. Although the
77 annual variation trend of total pollen amount generally exhibits a similar bimodal
78 pattern, increasing annual climatic variability amidst global warming has led to
79 significant changes in the pollen seasons of various plants, with discrepancies of more
80 than 20 days in some years. This variability poses practical challenges for conducting
81 pollen monitoring research and providing public meteorological services (He et al.,
82 2001; Gu and Liao, 2003; Bai et al., 2009; Lei et al., 2023). Therefore, studying
83 pollen concentration and distribution is crucial for understanding the pathogenesis of
84 airborne pollen diseases, conducting effective pollen monitoring research, and
85 delivering accurate public meteorological services.

86 However, compared to regions such as Europe and the United States, China faces
87 significant challenges in pollen monitoring due to fewer monitoring stations, shorter

88 monitoring histories, and a lower prevalence of automated facilities. These limitations
89 have resulted in China's pollen simulation research remaining primarily at the level of
90 simple statistical methods, focusing only on basic statistical studies of the impact of
91 meteorological conditions on pollen concentration. In contrast, numerical models are
92 rarely employed for regional simulation of pollen concentration. This situation
93 reflects the relative lag in China's pollen monitoring and research system, hindering a
94 deeper understanding of pollen dispersion patterns and the scientific study of related
95 health issues (Wu et al., 2011; Meng et al., 2016; Guan et al., 2021; Gao et al., 2022).

96 Although numerical models play a crucial role in simulating pollen concentration,
97 they require a clear understanding of pollen emissions. Numerical models are broad
98 mathematical frameworks used to simulate various physical processes through
99 numerical approximations, including atmospheric dynamics and climate systems. In
100 contrast, a pollen emission model specifically estimates the release and distribution of
101 pollen into the atmosphere, taking into account factors such as pollen phenology,
102 vegetation types, and environmental conditions. Pollen emissions are influenced not
103 only by meteorological factors but also by vegetation types, land use changes, and
104 human activities (Sofiev et al., 2006; Wozniak and Steiner, 2017; Zhang and Steiner,
105 2022; He et al., 2023; Lei et al., 2023). Particularly in the context of accelerated
106 urbanization, the selection and layout of urban greening plants have a significant
107 impact on pollen emissions. The complex interactions of these factors pose significant
108 challenges to accurately simulating pollen emissions.

109 Since 2004, various pollen prediction models have been developed to enhance
110 the accuracy of pollen emission estimates. Helbig et al. (2004) introduced a
111 parameterization method for calculating pollen release and resuspension fluxes,
112 implemented in the KAMM/DRAIS mesoscale model, although it relied on
113 assumptions due to limited observational data. Subsequently, Sofiev et al. (2006)
114 analyzed the feasibility of large-scale atmospheric migration of allergenic pollen,
115 validating existing dispersion models and providing key parameterizations for dry and
116 wet deposition, which were applied in Finland's SILAM (System for Integrated
117 modeLling of Atmospheric coMposition) system. However, this direct simulation of

118 pollen concentration based on numerical models has significant complexity and
119 uncertainty. Wozniak and Steiner (2017) developed the Pollen Emission Prediction
120 Model (PECM1.0), which simulates seasonal pollen counts based on geography,
121 vegetation, and meteorology. The model establishes empirical relationships between
122 historical average temperatures and pollen season timings for four vegetation types. It
123 captures up to 57% of seasonal variations, allowing for analysis of climate change
124 impacts on wind-driven pollen emissions. Building on this, Zhang and Steiner (2022)
125 introduced PECM2.0, which incorporates precipitation and CO₂ factors while refining
126 the linear relationship between annual pollen production and temperature, ultimately
127 predicting the temperature effects by the end of the century. However, the linear
128 relationships based on historical temperatures have significant uncertainties, limiting
129 their applicability for regional studies. Therefore, the challenge of constructing a
130 pollen emission model that is better suited for regional scales and has broader
131 applicability warrants careful consideration and further research. Such advancements
132 could significantly enhance our understanding of pollen dynamics and improve the
133 accuracy of related health risk assessments.

134 Given the importance of accurately modeling pollen emissions, validation of
135 numerical models for pollen emissions is necessary. These models not only provide a
136 framework for simulating atmospheric processes but also allow for a more nuanced
137 understanding of how various factors influence pollen dynamics. RegCM is the
138 pioneering regional climate model system used for climate downscaling, originating
139 in the late 1980s and early 1990s at the National Center for Atmospheric Research
140 (NCAR) in the USA. It has since undergone several development iterations and is
141 currently maintained at the International Centre for Theoretical Physics (ICTP) in
142 Italy. This open-source system is widely utilized by numerous research teams,
143 forming an extensive network for regional climate research. The model can be applied
144 globally and is evolving into a fully coupled regional earth system model,
145 incorporating ocean, lake, aerosol, desert dust, chemistry, hydrology, and land surface
146 processes. The version used in this study is RegCM4.7.1.

147 Therefore, this study constructs a pollen emissions model for the Beijing area,

148 leveraging pollen concentration and meteorological monitoring data, combined with
149 pollen phenology and the RF algorithm. It conducts a simulation study on the
150 emission phenology of three types of pollen in Beijing (Artemisia, Chenopod, and
151 total pollen concentration) to calculate the pollen emissions potential. The study also
152 investigates the seasonal and spatiotemporal distribution characteristics of pollen in
153 Beijing and its potential correlations with meteorological factors and climatic
154 conditions. Additionally, the constructed pollen emissions parameterization method is
155 applied to the RegCM and evaluated for accuracy using 15 years of pollen
156 observation data. This comprehensive study will enhance the understanding of pollen
157 sources, provide innovative guidance for the selection and planting of greening plants,
158 and promote sustainable development in ecological protection and urban planning.

159 **2. Methodology**

160 *2.1 Model description*

161 2.1.1 Parameterization method for pollen emissions

162 This study's pollen emissions potential integrates geographical parameters,
163 vegetation types, and meteorological data, and incorporates autumn pollen phenology
164 and RF to enhance the simulation of pollen phenology (Wozniak and Steiner, 2017;
165 Zhang and Steiner, 2022). This approach is used to predict pollen concentration and
166 distribution within the seasonal cycle. The specific calculation formula is as follows:

$$167 E_i(t) = f_i \bullet p_{annual,i} \bullet e^{-\frac{(t-\mu)^2}{2\delta^2}} \quad (1)$$

168 In the formula, $E_i(t)$ represents the pollen emissions potential for pollen type i on
169 day t of the year (DOY), t represents a specific day of the year, and i represents the
170 i -th type of pollen. f_i represents the vegetation land cover fraction, which is the
171 percentage of different vegetation types within a unit area, measured in %. $P_{annual,i}$
172 represents the production factor of the i -th vegetation type, which is the number of
173 pollen grains released during the pollen season, measured in $Grain\ m^{-2}\ year^{-1}$. In this
174 study, $P_{annual,i}$ is calculated based on the RF algorithm (Sect. 2.1.3). $e^{-\frac{(t-\mu)^2}{2\delta^2}}$

175 represents the phenological evolution of pollen emissions, controlling the pollen
 176 release process. The formula indicates that pollen emissions during the pollen season
 177 follows a Gaussian distribution, where μ and δ are the mean and standard
 178 deviation of the Gaussian distribution. These parameters are calculated from sDOY
 179 (start Day of Year) and eDOY (end Day of Year) of the pollen season, as follows:
 180

$$\mu = \frac{sDOY + eDOY}{2} \quad (2)$$

$$\delta = \frac{eDOY - sDOY}{a} \quad (3)$$

182 In this context, sDOY and eDOY are optimized using autumn pollen phenology
 183 (Sect. 2.1.2). The parameter a represents a fitting parameter that explains the
 184 conversion between the empirical phenological dates based on pollen count thresholds
 185 and the equivalent width of the emission curve. In this study, the value of a is set to 4.

186 This equation can be applied to a specific type of pollen or to the calculation of
 187 pollen concentration over the entire pollen season, depending mainly on the land
 188 cover type. The emission can be calculated offline using this equation or applied in
 189 online calculations.

190 2.1.2 Autumn pollen phenology model

191 In this study, we used three different calculation methods (Rs_1 , Rs_2 , Rs_{sig}) for the
 192 autumn phenology model to simulate sDOY and eDOY of autumn pollen (Meier &
 193 Bigler, 2023). Each model is related to temperature and SSH. The specific calculation
 194 formulas are as follows:

$$Rs_1 = \begin{cases} (T_{base} - T_i)^x \times (L_i / L_{base})^y, & T_i < T_{base} \wedge L_i < L_{base} \\ 0, & T_i \geq T_{base} \vee L_i \geq L_{base} \end{cases} \quad (4)$$

$$Rs_2 = \begin{cases} (T_{base} - T_i)^x \times (1 - L_i / L_{base})^y, & T_i < T_{base} \wedge L_i < L_{base} \\ 0, & T_i \geq T_{base} \vee L_i \geq L_{base} \end{cases} \quad (5)$$

$$Rs_{sig} = \frac{1}{1 + e^{a(T_i \times L_i - b)}} \quad (6)$$

$$\sum_{t_0}^{t_n} Rs_i \geq Y \quad (7)$$

199 In the above equations, Rs_1 , Rs_2 and Rs_{sig} represent three different autumn

phenology model categories. T_i and L_i represent the temperature and SSH on a given day, respectively, while T_{base} and L_{base} represent the thresholds for temperature and SSH, respectively. In the Rs_1 and Rs_2 models, when the temperature and SSH are below the threshold or the date exceeds a fixed DOY, Rs starts accumulating. In the Rs_{sig} model, temperature and SSH accumulate inversely in an exponential form. The day t_n , when the cumulative amount exceeds the threshold Y , represents the final simulated pollen start/end date. t_0 represents the start day of accumulation, which is the first day when $T < T_{base}$ and $L_i < L_{base}$. The parameters that need to be adjusted are Y , T_{base} , L_{base} , x , y and *start_day*. In this study, the simulated annealing (**SA**) algorithm is used for parameter adjustment. The principle of the **SA** is to simulate the random optimization process of the annealing process in solid-state physics, which can accept non-optimal solutions with a certain probability to avoid falling into local optima and eventually achieve the global optimum.

2.1.3 Random Forests

Random Forests (RF) is an ensemble learning algorithm introduced by Breiman (2001) for classification and regression tasks. This algorithm enhances model prediction performance and robustness by constructing multiple decision trees and combining their outputs. The core principle involves drawing multiple sample sets with replacement from the original training set, training a decision tree for each sample set, and randomly selecting a subset of features at each node split to reduce correlation between the trees. Ultimately, RF generates the final prediction by averaging (for regression) or voting (for classification) the outputs of these trees. The advantages of this method include high prediction accuracy, strong resistance to overfitting, suitability for high-dimensional data, and efficient training processes. The RF algorithm has been widely applied across various fields (Virro et al., 2022; Li et al., 2023; Chen et al., 2024; Valipour Shokouhi et al., 2024).

In this study, the RF algorithm is employed to simulate annual pollen production. Each pollen dataset is divided into training and testing sets in a 4:1 ratio, with the training set used for model training and the testing set for accuracy validation. Additionally, a grid search with cross-validation is applied to optimize the

230 hyperparameters of each estimator. Key parameters for RF adjustment include
 231 n_estimators, max_depth, min_samples_split, and min_samples_leaf. Hyperparameter
 232 optimization is a crucial step in enhancing model performance.

233 **2.1.4 Implementation of pollen emissions in RegCM**

234 In this model, a pollen emissions model based on phenology and RF calculates
 235 the emission potential of different types of pollen offline, and then incorporated into
 236 the RegCM model. The calculation of pollen concentration in this model follows the
 237 method of Sofiev et al. (2013), with the formula as follows:

$$238 \quad E_{pollen,i}(t) = E_i(t) \bullet f_w \bullet f_r \bullet f_h \quad (8)$$

$$239 \quad f_w = 1.5 - \exp(-(u_{10} + u_{conv})/5)$$

$$f_r = \begin{cases} 1, pr < pr_{low} \\ \frac{pr_{high} - pr}{pr_{high} - pr_{low}}, pr_{low} < pr < pr_{high} \\ 0, pr > pr_{high} \end{cases} \quad (9)$$

$$f_h = \begin{cases} 1, rh < rh_{low} \\ \frac{rh_{high} - rh}{rh_{high} - rh_{low}}, rh_{low} < rh < rh_{high} \\ 0, rh > rh_{high} \end{cases}$$

240 Where f_w , f_r and f_h represent the wind, precipitation, and RH factors,
 241 respectively, influencing pollen emissions concentration. f_w is exponentially related to
 242 the 10m wind speed u_{10} and vertical turbulent wind speed u_{conv} . pr and rh represent
 243 precipitation and RH. When precipitation is below the threshold pr_{low} , the
 244 precipitation factor is 1. When precipitation exceeds the threshold pr_{high} , the factor is 0.
 245 When precipitation is between these thresholds, the factor is calculated as the ratio of
 246 the difference between the high threshold and precipitation to the difference between
 247 the thresholds, with default values $pr_{low}=10^{-5}$ mm and $pr_{high}=0.5$ mm. Similarly, the
 248 RH factor is related to RH and its thresholds, with default values $rh_{low}=50$ % and
 249 $rh_{high}=80$ %. These factors explain the impact of wind, precipitation, and humidity on
 250 pollen emissions. Given the significant influence of precipitation and RH on pollen
 251 emissions, this study adjusts pr_{high} and rh_{high} values to 1 mm and 90 %, respectively.
 252 Higher thresholds can prevent excessive suppression of pollen emissions under

253 frequent precipitation and high humidity conditions, thus more accurately simulating
254 actual pollen concentration changes and better adapting the model to different climatic
255 conditions.

256 Moreover, the RegCM includes the pollen tracer transport equation (Solomon et al.
257 2006), as follows:

$$\frac{\partial \chi}{\partial t} = \bar{V} \cdot \nabla \chi + F_H + F_V + T_C + S - R_{Wls} - R_{Wc} - D_d \quad (10)$$

259 Where χ represents the tracer, F_H and F_V represent horizontal and vertical
260 diffusion, T_C represents convective transport, R_{Wls} and R_{Wc} represent large-scale and
261 convective precipitation wet removal processes, respectively, and D_d represents dry
262 removal processes. This transport equation comprehensively considers various
263 physical processes and removal mechanisms of pollen in the atmosphere, allowing the
264 simulation of the entire process from pollen release to atmospheric dispersion and
265 deposition. This provides a foundation for fully describing the spatial distribution and
266 temporal evolution of pollen in the atmosphere, which is crucial for studying pollen
267 dispersion in the air, determining the spatial distribution of pollen concentration, and
268 predicting future changes in pollen concentration.

269 2.2 Data

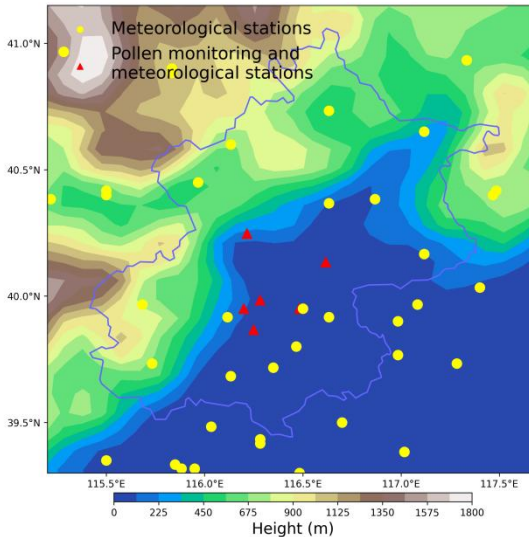
270 2.2.1 Observed pollen concentrations

271 The daily pollen concentration data were collected from six monitoring stations
272 in Beijing: Changping (CP), Chaoyang (CY), Fengtai (FT), Haidian (HD),
273 Shijingshan (SJS), and Shunyi (SY), as shown in Fig. 1. The monitoring period
274 spanned from April to October each year from 2006 to 2021, covering the main pollen
275 season in Beijing. The gravitational settling method (Unit: 10^3 Grains $m^{-2} d^{-1}$) was
276 used for monitoring. The pollen concentration data included Total Pollen
277 Concentration (the sum of pollen concentrations from all taxa, abbreviated as TotalPC)
278 and the concentrations of pollen from 10 common allergenic plants. These species
279 included trees such as Pine, Poplar, Birch, Cypress, Ash, and Elm, as well as weeds
280 like Artemisia, Chenopod, Humulus, and Amaranthus. Although autumn pollen
281 concentrations are lower compared to spring, autumn weed pollen has a higher

282 allergenic potential (Zhao et al., 2023). Therefore, this study focuses on the analysis
283 of autumn weed pollen. Due to significant data gaps in the pollen concentration of
284 specific species, we selected only the data that were more complete and of higher
285 allergenic potential, specifically Artemisia, Chenopod, and TotalPC. Table 1 provides
286 basic information, such as the number of effective sample years for these three types
287 of pollen across the six stations.

288 To prevent anomalies in the data, we excluded outliers in the pollen
289 concentration data for each species and any data points where the concentration
290 exceeded the 99th percentile. Furthermore, we applied a 5-day moving average to the
291 pollen monitoring data to smooth it. This approach not only eliminates noise from the
292 data (Li et al., 2019; Li et al., 2022) but also mitigates the influence of daily
293 meteorological changes and advection diffusion on daily pollen emissions (To further
294 analyze the impact of key factors such as meteorological factors and advection
295 diffusion on daily pollen emissions, we used the RegCM in Sect. 3.3. This model
296 accurately reflects the effects of daily meteorological factors such as temperature,
297 precipitation, humidity, and wind speed on pollen emissions while also describing key
298 physical processes such as advection diffusion, convective transport, and dry and wet
299 deposition, thus providing a comprehensive analysis of the behavior of pollen in the
300 atmosphere). This smoothing process allows us to more clearly explore the daily
301 variation trends of pollen.

302 Additionally, to better simulate the temporal and spatial distribution of pollen
303 during the autumn pollen period, we defined the autumn pollen period based on
304 observed pollen concentration data as $215 < \text{DOY} < 280$. Subsequently, we
305 determined the sDOY and eDOY for the autumn pollen period for each station and
306 year by identifying the day of year at which the cumulative pollen concentration
307 reached 5 % (start) and 95 % (end) of the total for that period (Khwarahm et al., 2017;
308 Li et al., 2019; Li et al., 2022).



309

310 Fig. 1. Distribution map of geopotential height, pollen observation stations (triangle), and
 311 meteorological monitoring stations (circle) in Beijing area

312 Table 1 Explanation of effective sample years for pollen monitoring stations in Beijing

313 (2006-2021)

Station	Effective Sample Years / Year		
	Artemisia	Chenopod	TotalPC
CP	16	16	16
CY	13	13	13
FT	10	8	15
HD	0	0	8
SJS	11	11	16
SY	12	9	16
Total	62	57	84

314 To better simulate sDOY and eDOY for pollen, this study first applied the
 315 Gaussian model to the autumn pollen data of each station and year. The Gaussian
 316 model was chosen for its effectiveness in capturing peaks in time series data, which
 317 are often reflected in pollen concentration data. Taking the CP station as an example,
 318 Gaussian fitting distribution was performed on the autumn Artemisia, Chenopod, and
 319 TotalPC for 2006-2021 (Supplementary Fig. S1-S3). The results indicated that the
 320 autumn pollen concentration exhibited a significant Gaussian distribution, confirming
 321 that the Gaussian model could aptly fit the time series changes of autumn pollen.

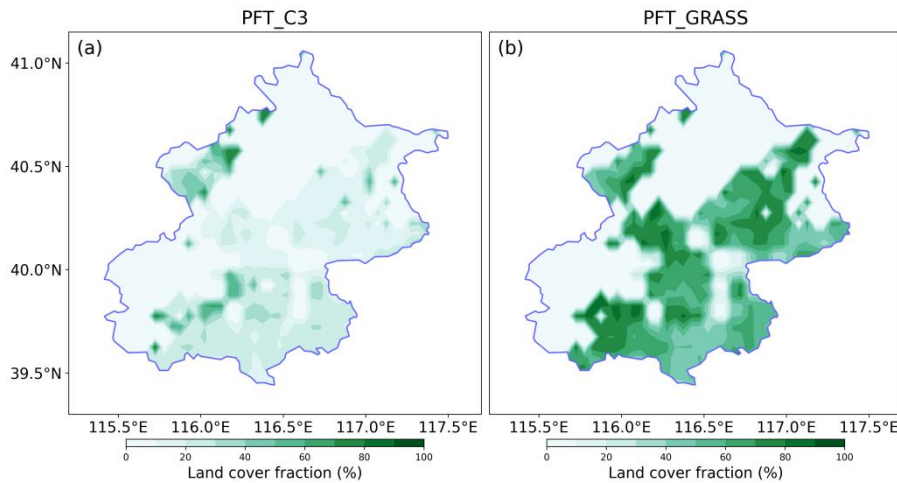
322 Therefore, by Gaussian fitting the pollen concentrations of each station, the autumn
323 pollen sDOY and eDOY under the Gaussian model simulation were further
324 determined. Comparing the sDOY and eDOY derived from observed pollen
325 concentration data with those obtained via Gaussian model simulation
326 (Supplementary Fig. S4), we found a high correlation coefficient (R) and a low root
327 mean square error (RMSE) between the two. Thus, the sDOY and eDOY obtained
328 from Gaussian model simulation were utilized to study the autumn pollen phenology.

329 *2.2.2 Meteorological observation and land cover data*

330 The meteorological data for this study were sourced from the China Surface
331 Climate Daily Dataset, encompassing observations from all benchmark and basic
332 meteorological stations in China. Specifically, we utilized data from 66 valid
333 meteorological stations in Beijing and its surrounding areas (39-41.5° N, 115-118° E)
334 covering the period from 2006 to 2020 (Fig. 1). This dataset includes meteorological
335 observations corresponding to the pollen monitoring stations (our meteorological data
336 extends only up to 2020). The variables incorporated in this study comprise average
337 temperature (TEM_Avg), maximum temperature (TEM_Max), minimum temperature
338 (TEM_Min), sunshine hours (SSH), station altitude (Alti), average pressure
339 (PRS_Avg), maximum pressure (PRS_Max), minimum pressure (PRS_Min),
340 maximum wind speed (WIN_S_Max), extreme wind speed (WIN_S_Inst_Max),
341 average 2-minute wind speed (WIN_S_2mi_Avg), ground surface temperature
342 (GST_Avg_Xcm, X=5, 10, 15, 20, 40, 80, 160, 320cm), average ground surface
343 temperature (GST_Avg), minimum ground surface temperature (GST_Min),
344 maximum ground surface temperature (GST_Max), average relative humidity
345 (RHU_Avg), minimum relative humidity (RHU_Min), average vapor pressure
346 (VAP_Avg), precipitation from 20:00 to 20:00 (PRE_Time_2020), and precipitation
347 from 08:00 to 08:00 (PRE_Time_0808). The first four meteorological factors were
348 utilized to simulate the autumn phenology model of pollen, predicting various pollen
349 sDOY and eDOY. All meteorological factors served as training datasets for the RF
350 algorithm to simulate annual pollen production.

351 For land use data, this study employed the Community Land Model 4 (CLM4)

352 dataset (Oleson et al., 2010), which includes 25 plant functional types such as
 353 needleleaf forests, broadleaf forests, shrubs, grasses (C3 and C4), and crops, with a
 354 spatial resolution of 0.05° . As *Artemisia* and *Chenopod* primarily fall under the C3
 355 plant category (Yorimitsu et al., 2019; Septembre-Malaterre et al., 2020; Qiao et al.,
 356 2023), the simulation of pollen utilization for *Artemisia* and *Chenopod* used plant
 357 functional C3 grass, while the TotalPC simulation incorporated both C3 and C4
 358 grasses. The distribution of these two plant functional types in Beijing is illustrated in
 359 Fig. 2.



360
 361 Fig. 2. The distribution of plant functional type C3 (a) and GRASS (b) in Beijing area

362 3. Results and Discussion

363 3.1 Pollen Phenology Simulation

364 In this study, we analyzed the phenological changes of three types of
 365 pollen—*Artemisia*, *Chenopod*, and TotalPC—during the autumn season based on
 366 three different autumn pollen phenology calculation methods (Rs_1 , Rs_2 , and Rs_{sig}).
 367 Specifically, we examined the seasonal phenological simulations of these pollen
 368 concentrations under three different temperature conditions (TEM_Avg, TEM_Max,
 369 and TEM_Min) (Mo et al., 2023), with a primary focus on sDOY and eDOY.
 370 Additionally, the annual pollen production (P_{annual}) was simulated using the RF
 371 algorithm.

372 3.1.1 Simulation of sDOY and eDOY based on autumn phenology model

373 Table 2 presents the statistical indicators for simulating the phenology of

374 Artemisia using different phenological methods and temperature conditions. For
375 simulating the sDOY for Artemisia, the Rs_1 , Rs_2 , and Rs_{sig} methods demonstrated high
376 accuracy when TEM_Avg and TEM_Min were employed as temperature conditions.
377 The R values for both the training and testing sets exceeded 0.45, with some R values
378 in the testing set surpassing 0.7, and the RMSE values were relatively low. This
379 indicates that these three methods effectively capture the phenological characteristics
380 of Artemisia at the onset of autumn. Notably, the Rs_{sig} method, when using TEM_Avg
381 as the condition, achieved R values of 0.53 and 0.80 for the training and testing sets,
382 respectively, with RMSE values of 6.61 days and 4.86 days, showing the best
383 simulation performance. However, when TEM_Max was used as the temperature
384 condition, the simulation performance of all three methods declined. The R value of
385 the Rs_1 method fell below 0.2, and the RMSE values were high, exceeding 8 days.
386 Comparatively, the Rs_{sig} method performed slightly better but still yielded inferior
387 results compared to TEM_Avg and TEM_Min, indicating lower model stability when
388 predicting Artemisia sDOY with TEM_Max. For the simulation of Artemisia eDOY,
389 the performance of the three methods was relatively close, with R values in the
390 training and testing sets generally ranging from 0.3 to 0.5, and similar RMSE values.
391 Among them, the Rs_1 method performed better when TEM_Min and TEM_Avg were
392 used as temperature conditions, with R values of 0.66 and 0.51 in the testing set and
393 RMSE values of 3.32 days and 3.9 days, respectively. Compared to the Rs_1 method,
394 the Rs_2 and Rs_{sig} methods were relatively weaker in predicting eDOY, indicating that
395 the Rs_1 method better captures the phenological trends of Artemisia at the end of
396 autumn. Additionally, when comparing the simulation results of sDOY and eDOY,
397 sDOY generally had higher R values, but eDOY had lower overall RMSE values.

398 The statistical indicators for simulating the phenology of Chenopod under
399 different phenological methods and temperature conditions are shown in Table S1. For
400 the simulation of the sDOY for Chenopod, the Rs_1 and Rs_2 methods demonstrated
401 high accuracy when using TEM_Min and TEM_Avg as temperature conditions. The R
402 values for both the training and testing sets were around 0.5, and the RMSE values
403 were relatively low. It is clear that using TEM_Avg as the temperature condition

404 yields higher R values and lower RMSE (in the case of the Rs_1 method) compared to
405 TEM_{Min} , indicating that these two methods effectively capture the phenological
406 changes of Chenopod at the onset of autumn when using TEM_{Avg} as the
407 temperature condition. However, when TEM_{Max} was used as the temperature
408 condition, the simulation performance of all three methods declined, particularly for
409 Rs_1 , which had an R value of -0.1 and an RMSE greater than 9 days in the testing set.
410 The Rs_{sig} method, when using TEM_{Avg} , achieved an R value of 0.51 in the training
411 set but only 0.28 in the testing set, with a high RMSE of 5.32 **days**, indicating poor
412 model stability in this scenario. In contrast to TotalPC and Artemisia, the simulation
413 of the eDOY for Chenopod was not satisfactory for any of the three methods. The R
414 values for both the training and testing sets were all below 0.42. Particularly when
415 using TEM_{Max} as the temperature condition, the simulation performance of all three
416 methods was poor, with the testing set R value reaching only 0.1. This indicates that
417 the models have limited ability to capture the end of the autumn season for Chenopod.

418 Table **S2** shows the phenological simulation statistical indicators of TotalPC
419 under different phenological methods and temperature conditions. From the data in
420 the table, it can be seen that for the simulation of the sDOY of TotalPC, all three
421 phenological methods (Rs_1 , Rs_2 , and Rs_{sig}) performed with high accuracy ($R > 0.5$)
422 and relatively low RMSE when using TEM_{Min} . This indicates that these three
423 methods, when using TEM_{Min} , can effectively capture the trend of the sDOY of
424 TotalPC during the autumn season. Meanwhile, the Rs_1 method also showed good
425 simulation performance when using TEM_{Avg} as the temperature condition, with R
426 reaching 0.54 for both the training and testing sets. The Rs_{sig} method, using TEM_{Avg} ,
427 had good simulation performance in the training set, but the R in the testing set only
428 reached 0.38. Compared to TEM_{Min} and TEM_{Avg} , the Rs_2 and Rs_{sig} methods
429 showed slightly inferior simulation performance when using TEM_{Max} as the
430 temperature condition. Surprisingly, the Rs_1 method's simulation of the sDOY showed
431 a negative correlation when using TEM_{Max} , indicating the worst performance. For
432 the simulation of the eDOY of TotalPC, the overall simulation performance was
433 worse in terms of R compared to sDOY, but the RMSE values were generally better.

434 Specifically, using TEM_Avg as the temperature condition, the Rs₂ and Rs_{sig} methods
 435 showed relatively good simulation performance and lower RMSE. However, the Rs₂
 436 method performed much worse on the testing set compared to the training set, with
 437 the R on the testing set being only 0.32.

438 Overall, different pollen types exhibit varying sensitivity to different
 439 phenological models and temperature conditions. TEM_Avg is generally the best
 440 temperature condition for predicting the sDOY of the three pollen types, providing
 441 higher R values and lower RMSE. This suggests that TEM_Avg can effectively
 442 predict the start of the autumn pollen season. At the same time, TEM_Min also
 443 performs well in predicting the sDOY of TotalPC and Artemisia, whereas TEM_Max
 444 generally shows the poorest prediction performance. For predicting eDOY, different
 445 pollen types show different sensitivities to temperature conditions, but overall, the
 446 models perform worse for eDOY compared to sDOY, especially in the simulation of
 447 Chenopod.

448 Table2 Statistical indicators of Artemisia phenology under different phenological methods and
 449 temperature conditions. (Unit of RMSE: day)

	Artemisia	Rs ₁ (R)		Rs ₂ (R)		Rs _{sig} (R)		Rs ₁ (RMSE)		Rs ₂ (RMSE)		Rs _{sig} (RMSE)	
		Train	Test	Train	Test	Train	Test	Train	Test	Train	Test	Train	Test
sDOY	TEM_Min	0.47	0.66 [#]	0.52*	0.77 [#]	0.45	0.59 [#]	6.61	5.93	6.29	4.99	6.63	6.57
	TEM_Avg	0.45	0.63 [#]	0.50	0.71 [#]	0.53*	0.80[#]	6.67	6.18	6.78	5.44	6.61	4.86
	TEM_Max	0.16	0.17	0.44	0.47	0.45	0.58 [#]	8.87	9.58	8.21	7.51	6.52	6.32
eDOY	TEM_Min	0.38	0.66[#]	0.38	0.44	0.36	0.37	4.19	3.32	4.19	3.97	4.02	4.07
	TEM_Avg	0.46	0.51*	0.38	0.29	0.44	0.44	3.92	3.9	4.16	4.23	3.85	4.07
	TEM_Max	0.31	0.43	0.05	0.07	0.33	0.27	5.59	4.65	6.84	6.47	3.98	4.32

450 Note: Bold represents the best model performance, [#] Indicates significance levels at P < 0.001, *
 451 Indicates significance levels at P < 0.005

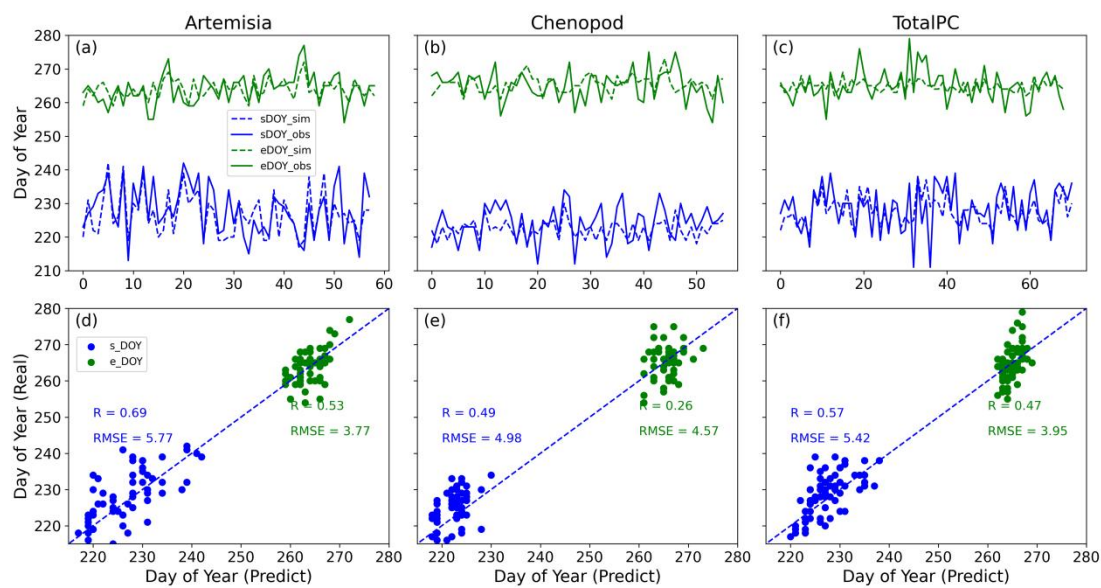
452 Based on the above discussion, we selected the most suitable phenological and
 453 temperature conditions for the three types of pollen (bold parts in Table 2 and Table
 454 S1-S2), simulated their sDOY and eDOY, and generated line and scatter plots (Fig. 3).

According to the line plots in Fig. 3 (top), the predicted results for Artemisia are the closest to the actual observed results. The predictions for TotalPC follow, while the predictions for Chenopod show some deviation, particularly in eDOY, indicating the need for a more suitable phenological model to accurately simulate the phenology of Chenopod. The scatter plots in Fig. 3 (bottom) illustrate that for sDOY predictions, Artemisia exhibited the strongest correlation between predicted and observed pollen phenology, with an R value of 0.69 and an RMSE of 5.77 days. In contrast, Chenopod had the lowest correlation, with an R value of 0.49 and an RMSE of 4.98 days. It can also be observed that higher R values are associated with higher overall RMSE, possibly due to the models being more sensitive to noise or outliers in the data, which increases the overall error. For high-correlation predictions like those for Artemisia, the model may be more affected by random fluctuations in the data, leading to increased error. Additionally, different pollen types may exhibit varying characteristics or response patterns in phenological models, resulting in a non-linear or inconsistent relationship between correlation and error. For eDOY predictions, the correlation between predicted and observed is highest for Artemisia, with an R value of 0.53 and an RMSE of 3.77 days. Chenopod has the lowest correlation for eDOY predictions, with an R value of only 0.26 and an RMSE of 4.57 days. The poorer performance in simulating eDOY for Chenopod may be due to lower data quality compared to Artemisia and TotalPC, as well as the smallest sample size, resulting in insufficient information and samples for the model to learn and predict accurately.

Additionally, Table 3 shows the proportion of simulations with errors less than 5 days and 3 days for sDOY and eDOY across the three pollen types. It can be seen that the proportion of eDOY simulations with errors less than 5 days and 3 days is higher than that for sDOY, indicating that eDOY simulations generally have better accuracy in terms of error. Specifically, for Chenopod eDOY simulations, although the R value is poor, 76.79 % of simulations have errors less than 5 days, and 55.36 % have errors less than 3 days, meaning that more than half of the eDOY simulations have errors within 3 days. This performance is comparable to the other two pollen types (64.41 % and 68.12 %, respectively). Compared to Mo et al. (2023), which simulated the spring

485 season start pollen season (SPS) using 17 phenological models, this study has slightly
 486 lower R values but much lower RMSE (around 11 days in their study). Li et al. (2022)
 487 used satellite data to simulate the SPS for Birch, Oak, and Poplar, achieving RMSE
 488 values between 4.26 and 8.77 days. Furthermore, this study's process-based
 489 phenological models for sDOY and eDOY show smaller errors and higher
 490 correlations compared to empirical linear models based solely on temperature used by
 491 Wozniak and Steiner (2017) and Zhang and Steiner (2022).

492 Therefore, from an error analysis perspective, the simulation performance of
 493 Chenopod eDOY maintains a relatively low error while also demonstrating some
 494 stability, indicating that the autumn phenological model can accurately capture the
 495 seasonal variation trend of Chenopod. This makes the simulation results reliable.
 496 Overall, the autumn phenological models provide good simulation performance for
 497 the phenology of the three pollen types, laying a solid foundation for further analysis
 498 of pollen temporal characteristics.



499
 500 Fig. 3. Comparison of pollen sDOY and eDOY in autumn phenology: simulation vs. observation.
 501 Line plots of three different pollen sDOY and eDOY (a-c) and scatter plot comparison of the same
 502 (d-f). Specific comparisons for Artemisia (a, d), Chenopod (b, e), and TotalPC (c, f). **The**
 503 **horizontal axis of (a-c) represents the sequential distribution of effective sample counts for the**
 504 **three types of pollen.**

505 Table3 Statistics on the proportion of errors between simulation and observation of three different

506

types of pollen sDOY and eDOY within 5 and 3 days

	DOY	Artemisia (%)	Chenopod (%)	TotalPC (%)
<5D	sDOY	68.97	73.21	71.83
	eDOY	86.44	76.79	82.61
<3D	sDOY	48.28	44.64	53.52
	eDOY	64.41	55.36	68.12

507

Based on the temperature and SSH observational station data from the Beijing area, we interpolated the station data into a grid dataset with a horizontal resolution of 0.1°. Using the selected autumn phenological models, we then performed gridded simulations of the sDOY and eDOY for three pollen types. This approach enabled us to map the regional distribution of autumn pollen sDOY and eDOY in Beijing from 2006 to 2020, thereby laying the groundwork for further simulations of autumn pollen emissions potential.

514

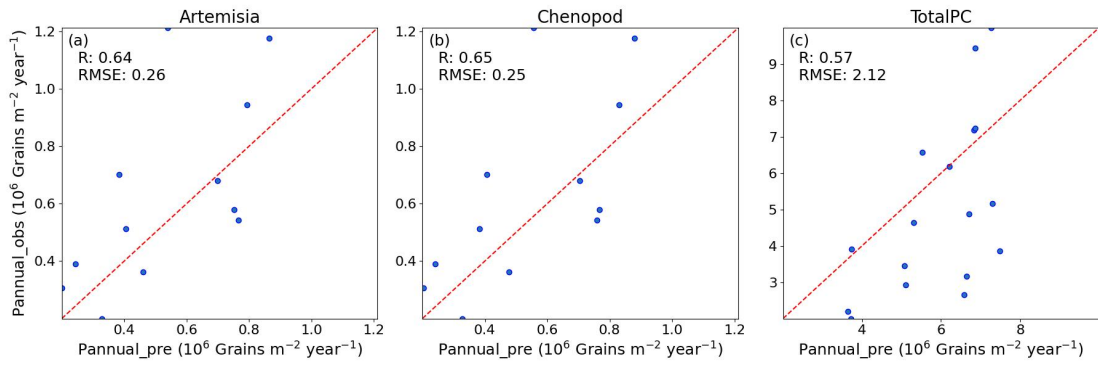
3.1.2 Simulation of annual pollen production based on RF

515

The simulation of annual pollen production (P_{annual} , referring to the cumulative pollen concentration during each autumn pollen season) was conducted using the RF algorithm. The training data comprised all station-observed pollen data from Table 1 and the corresponding meteorological observation data from Sect. 2.2.2. Four-fifths of the station data were randomly selected as the training set to train the RF algorithm, while the remaining one-fifth was used as the test set to validate the accuracy of the RF's P_{annual} simulation. Fig. 4 presents the scatter plots of observed versus simulated P_{annual} for three different pollen types (Artemisia, Chenopod, and TotalPC) based on the RF in the test set. The R between simulated and observed values for the three pollen types were all above 0.5, with Chenopod reaching 0.65. The calculated RMSE was around 0.2×10^6 Grains m⁻² year⁻¹ (with TotalPC having an RMSE of 2.12×10^6 Grains m⁻² year⁻¹). This indicates that the prediction performance of the RF varies among different pollen types, with the best performance for Chenopod and the poorest for TotalPC annual production. Compared to the temperature-based empirical linear

529 models for P_{annual} by Zhang and Steiner (2022), the machine learning algorithm-based
 530 simulations in this study have smaller errors and higher correlations. Overall, the RF
 531 effectively simulates P_{annual} .

532 Based on meteorological observation data from stations in and around Beijing,
 533 the station data were interpolated into a gridded dataset with a horizontal resolution of
 534 0.1° . Subsequently, all station data for each pollen type were used as the training set,
 535 with 12 stations in the gridded dataset cyclically selected as the test set for gridded
 536 simulations. This ultimately resulted in the spatial distribution of P_{annual} in Beijing
 537 from 2006 to 2020, laying the foundation for further simulation of autumn pollen
 538 emissions potential.



539
 540 Fig. 4. Scatter plots of simulated and observed annual pollen (P_{annual}) based on RF. Comparisons
 541 for Artemisia (a), Chenopod (b), and TotalPC (c).

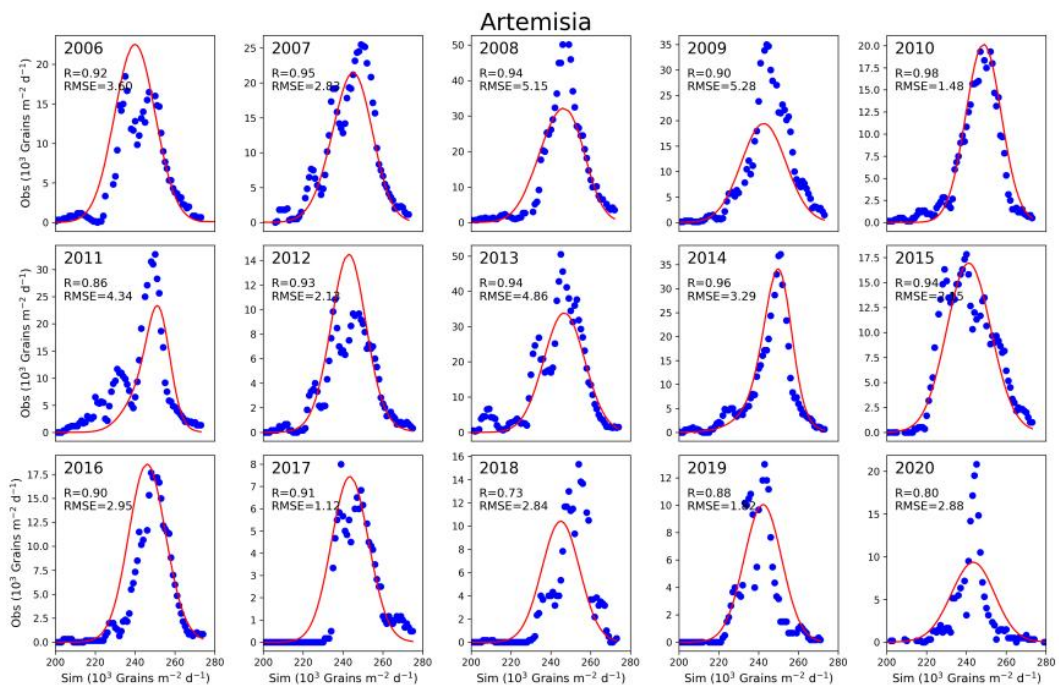
542 3.2 Simulation of Pollen Emissions in Beijing Area

543 Based on the simulation results of autumn pollen phenology (sDOY, eDOY, and
 544 P_{annual}) from Sect. 3.1 and the pollen emissions potential parameterization method
 545 from Sect. 2.1.1, this study calculated the pollen emissions potential in the Beijing
 546 area. Fig. 5 and Fig. S5-S6 present a comparison between the observed and simulated
 547 average site values of Artemisia, Chenopod, and TotalPC in Beijing from 2006 to
 548 2020. In these figures, blue dots represent the actual daily observed pollen counts, and
 549 red lines represent the simulated pollen emissions. To assess the consistency between
 550 the simulated and observed data, we calculated R and RMSE. As illustrated in the
 551 figures, the simulated data closely match the actual observations in most years, with
 552 correlation coefficients around 0.9. Specifically, the Artemisia emissions in 2010,
 553 Chenopod emissions in 2016, and TotalPC emissions in 2007, 2009, 2018, and 2019

554 show R values as high as 0.98 and relatively low RMSE levels, demonstrating the
 555 high accuracy of this study in simulating pollen emissions potential.

556 Additionally, the simulation results for sDOY and eDOY were also satisfactory,
 557 though there were slight advances in the start of the pollen season in certain years,
 558 such as 2017 and 2018 for Artemisia and Chenopod. While the peak pollen emissions
 559 simulations were highly accurate in most years, there were instances of
 560 overestimation and underestimation in some years. For example, the peak emissions
 561 of Artemisia in 2008, 2009, and 2020, Chenopod in 2007, and TotalPC in 2013 and
 562 2020 were significantly underestimated. Conversely, the peak simulations of TotalPC
 563 in 2011 and 2012 were slightly overestimated. This indicates that, despite the high
 564 accuracy of the annual pollen production simulations based on the RF, there is still
 565 room for improvement

566 Overall, this study achieved significant results in simulating pollen emissions,
 567 demonstrating the potential application of autumn phenological models and the RF
 568 algorithm in simulating pollen emissions. However, to further enhance the accuracy of
 569 these simulations, future research needs to investigate and address the instances of
 570 overestimation and underestimation in greater detail.



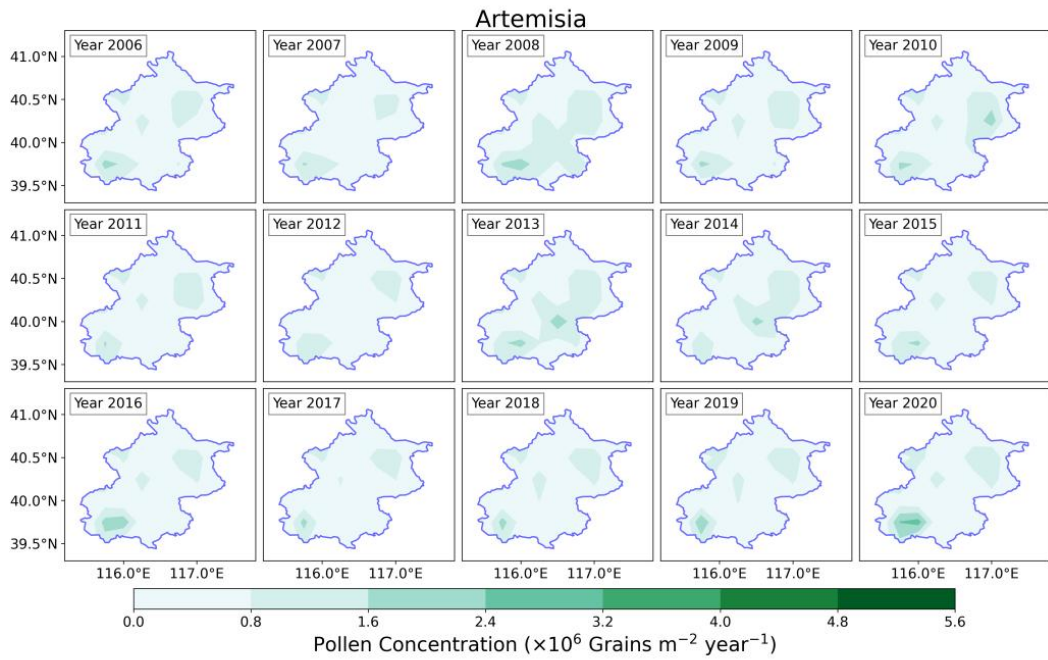
571

572 Fig. 5. Time series of observation and simulation of average Artemisia emissions at stations in

573 Beijing from 2006 to 2020. The red solid line represents the simulation of pollen emissions model,
574 while blue dots depict observations

575 To further investigate the spatial distribution of annual pollen production, we
576 simulated the spatial distribution of annual Artemisia, Chenopod, and TotalPC
577 production in Beijing from 2006 to 2020 (Fig. 6 and Fig. S7-S8). The results reveal
578 significant spatial and temporal variations in annual pollen production. Spatially,
579 Artemisia production is predominantly concentrated in the southeastern, northeastern,
580 and certain northwestern regions of Beijing, with occasional occurrences in the central
581 urban area during specific years (2008 and 2013). Chenopod production is highest in
582 the southern part of Beijing and lowest in the northern parts and surrounding areas.
583 Notably, from 2006 to 2008, the southern region exhibited high concentrations of
584 Chenopod production. TotalPC is mainly distributed in the southeastern plains of
585 Beijing, forming a strip-like pattern, while lower production is observed in the
586 northwestern mountainous areas, indicating a possible influence of geographical
587 location on TotalPC distribution. Temporally, the annual production of these three
588 pollen types demonstrates distinct interannual variations. Artemisia shows little
589 change in both distribution area and production concentration over time. In contrast,
590 Chenopod and TotalPC exhibit a general declining trend, reaching their lowest levels
591 between 2016 and 2018, which may be attributed to recent climatic changes,
592 vegetation shifts, and human activities in the Beijing area.

593 The simulation results for annual pollen production of Artemisia, Chenopod, and
594 TotalPC in Beijing from 2006 to 2020, based on autumn phenology and the RF pollen
595 emissions model, indicate pronounced spatial differences and temporal variation
596 characteristics. Analyzing the spatial distribution and temporal variation of annual
597 pollen production in Beijing enhances our understanding of the spatiotemporal
598 patterns of pollen in the region, providing crucial insights for the control and
599 mitigation of pollen allergies.



600

601 Fig. 6. Distribution of Artemisia in Beijing from 2006 to 2020 based on pollen emissions model

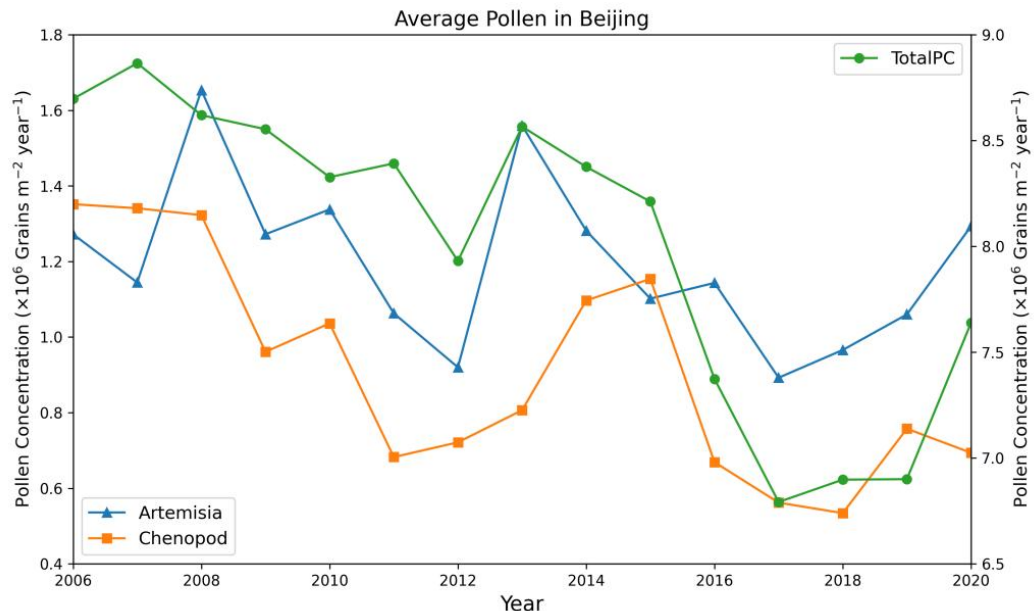
602 To more intuitively reflect the temporal variation trends in the annual production
 603 of three types of pollen, we further analyzed the interannual variation of the regional
 604 average cumulative concentration of these pollen types during the autumn pollen
 605 season in Beijing from 2006 to 2020 (Fig. 7). The annual production of Artemisia,
 606 Chenopod, and TotalPC in Beijing averages between 0.8-1.6, 0.5-1.4, and 6.5-9 grains
 607 $\text{m}^{-2} \text{ year}^{-1}$, respectively. The annual production of Artemisia and Chenopod are
 608 notably similar. Over time, the regional annual production of these pollen types in
 609 Beijing exhibits significant fluctuations. Nonetheless, Artemisia remains relatively
 610 stable, whereas Chenopod and TotalPC production demonstrate a discernible
 611 declining trend, particularly in TotalPC. The annual production of all three pollen
 612 types reached a local nadir in 2012. Following a surge in 2013, production steadily
 613 declined from 2014 to 2017, reaching the lowest levels observed in nearly 15 years
 614 (with TotalPC being the lowest in 2018). Subsequently, from 2018 to 2020, an
 615 increasing trend was observed. Overall, the annual pollen production in Beijing
 616 appears to follow a minor cyclical pattern, intimately linked to the impacts of climate
 617 change. **Building on this analysis, it suggest that interannual variations in pollen**
 618 **production may be influenced by multiple climate-related factors, such as temperature,**

619 precipitation, and SSH. These climatic elements can influence the phenology and
620 growth cycles of pollen-producing plants, thereby affecting their annual production
621 levels. For example, higher temperatures may lead to earlier flowering times,
622 potentially shifting the timing and duration of pollen release. Variations in
623 precipitation impact soil moisture, which can affect plant health and, consequently,
624 pollen output. The observed trends in Beijing's pollen production, including the
625 declining patterns in Chenopod and TotalPC, could correspond to climate shifts that
626 are less favorable for these species. Thus, these fluctuations in pollen production
627 underscore the sensitivity of pollen phenology to both local and broader climate
628 variations.

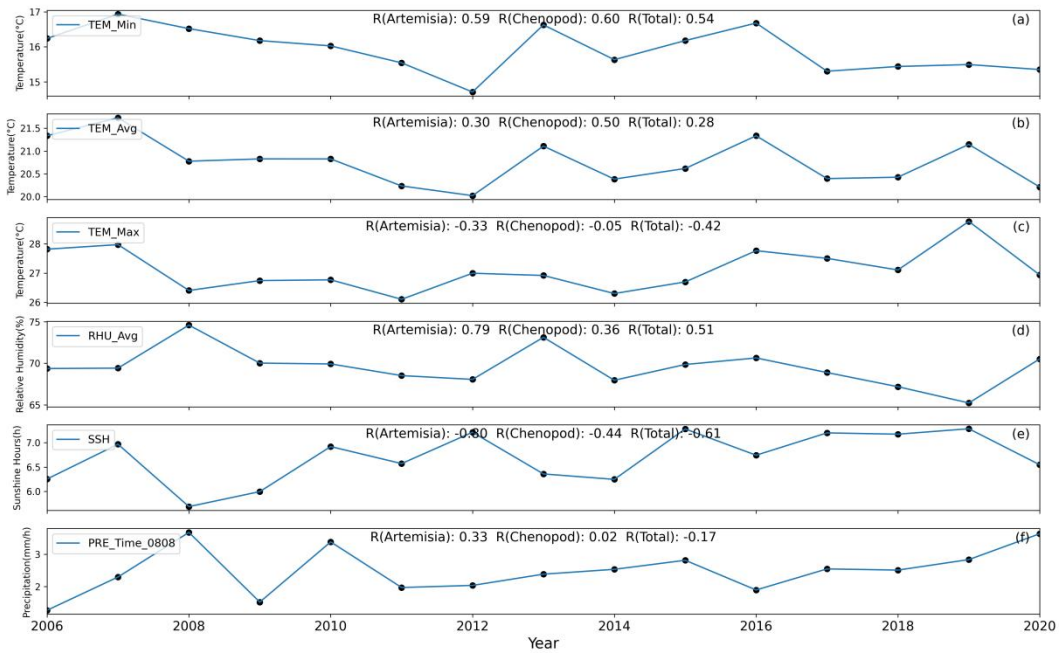
629 To further explore the meteorological factors influencing average annual pollen
630 production in Beijing, we selected six meteorological variables during the autumn
631 pollen season from 2006 to 2020 for temporal and regional average calculations.
632 These factors include maximum temperature (TEM_Max), average temperature
633 (TEM_Avg), minimum temperature (TEM_Min), average relative humidity
634 (RHU_Avg), sunshine hours (SSH), and precipitation time (PRE_Time_0808). The
635 annual variations of these meteorological factors were analyzed, and their correlations
636 with annual pollen production variations were calculated (Fig. 8).

637 The trends in annual variations of each meteorological factor and the calculated
638 correlations reveal that for Artemisia, TEM_Min and RHU_Avg have a significant
639 positive correlation with its production, especially RHU_Avg, which shows a
640 correlation of 0.79. This indicates that an increase in relative humidity promotes
641 Artemisia production. Conversely, SSH has a correlation of -0.8 with Artemisia,
642 indicating that longer sunshine hours inhibit its production. Meanwhile, TEM_Avg
643 and PRE_Time_0808 have minor promoting effects on Artemisia production, while
644 TEM_Max has a slight inhibitory effect. For Chenopod, TEM_Min is the most
645 significant promoting factor, while SSH has an inhibitory effect, although its negative
646 correlation is lower than that for Artemisia, indicating a limited inhibitory effect on
647 Chenopod production. For TotalPC, similar to Artemisia, increases in TEM_Min and
648 RHU_Avg promote production, while increases in SSH and TEM_Max inhibit

649 production. Notably, the three types of pollen reached local minimum concentrations
 650 in 2012, 2017, and 2018, when TEM_Min and SSH respectively reached local
 651 minimum and maximum values, further demonstrating the promoting effect of
 652 TEM_Min and the inhibitory effect of SSH on annual average pollen concentration.
 653 Rahman et al. (2020) and Lei et al. (2023) indicated that temperature is the main
 654 factor affecting the interannual variation of pollen and is positively correlated with
 655 pollen production. Our findings are largely consistent with these conclusions,
 656 although they did not consider the effect of SSH on interannual changes in pollen
 657 concentration. In summary, the annual production of pollen in Beijing is significantly
 658 influenced by meteorological conditions, particularly temperature, relative humidity,
 659 and sunshine hours. Different meteorological factors exhibit distinct promoting and
 660 inhibiting effects on pollen production.



661
 662 Fig. 7. Time series variation chart of regional average annual production of three types of pollen in
 663 Beijing from 2006 to 2020. Due to the different magnitudes of pollen concentrations, the left
 664 y-axis represents the concentrations of Artemisia and Chenopod, while the right y-axis represents
 665 TotalPC. Plotting the time series distributions of the three pollen concentrations on a single graph
 666 allows for a clearer observation of the trends in their variations over time.

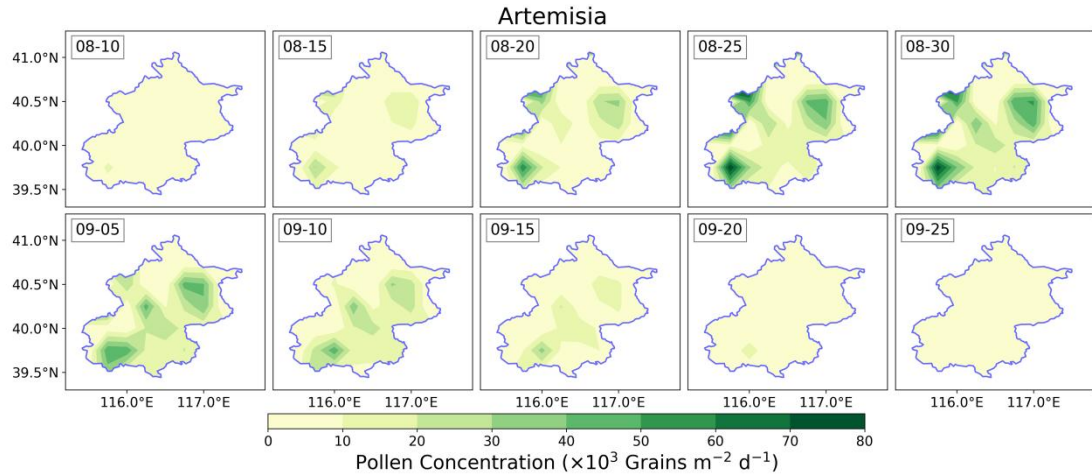


667

668 Fig. 8. Time series variation chart of average values of different meteorological factors in Beijing
 669 from 2006 to 2020. (The correlation coefficient between the average meteorological factors and
 670 the regional average annual production of three types of pollen is calculated in the figure)

671 Fig. 9 and Fig. S9-S10 illustrate the spatial distribution of the average
 672 concentrations of Artemisia, Chenopod, and TotalPC during the autumn pollen season
 673 in Beijing from 2006 to 2020. During this period, the concentration of all three pollen
 674 types initially increases and then decreases. The pollen season begins around August
 675 10 each year and concludes around September 25. The peak concentrations for
 676 Artemisia and Chenopod pollen occur around August 30, while the peak concentration
 677 for TotalPC is observed around September 5. The entire pollen season lasts
 678 approximately 45 days.

679 Regarding the average pollen concentration distribution, Artemisia is primarily
 680 concentrated in the southwest, northeast, and parts of the northwest of Beijing, with
 681 lower concentrations in the southeast. In contrast, Chenopod and TotalPC are mainly
 682 distributed in the southeastern plains. The maximum average concentrations for
 683 Artemisia, Chenopod, and TotalPC reach 81.1×10^3 Grains $m^{-2} d^{-1}$, 42.0×10^3 Grains
 684 $m^{-2} d^{-1}$, and 351.8×10^3 Grains $m^{-2} d^{-1}$, respectively.



685

686 Fig. 9. Temporal and spatial distribution of Artemisia in Beijing (average from 2006 to 2020)

687 *3.3 Simulation of Pollen Emissions in Regional Climate Models*

688 To evaluate the pollen emissions model based on autumn pollen phenology and
 689 RF, this study integrates the offline calculated pollen emissions into the regional
 690 climate model RegCM. By comparing the simulated atmospheric pollen
 691 concentrations with data from ground-based pollen monitoring stations, we assess the
 692 performance of this pollen emissions potential model.

693 *3.3.2 Evaluation of pollen simulation accuracy in RegCM*

694 Fig. 10 and Fig. S11-S12 depict the time series distribution of the concentrations
 695 of three pollen types simulated by the RegCM compared to observed concentrations
 696 from 2006 to 2020. The RegCM successfully captures the temporal variation trends of
 697 pollen concentrations during the autumn pollen season, generally showing an initial
 698 increase followed by a decrease. Daily pollen concentrations fluctuate significantly
 699 due to meteorological factors such as temperature, precipitation, and RH, as well as
 700 key physical processes like advection, convection, and dry and wet deposition.
 701 Overall, the simulated pollen concentrations by the RegCM align well with the
 702 observed trends, though some discrepancies remain.

703 In the simulation of Artemisia (Fig. 10), the sDOY and pollen production vary
 704 annually due to meteorological conditions and key physical processes. The annual
 705 peak pollen concentrations generally range from $20-70 \times 10^3$ Grains $m^{-2} d^{-1}$, while in
 706 2019-2020, observed pollen concentrations exceeded 100×10^3 Grains $m^{-2} d^{-1}$, with
 707 notable spikes and drops likely due to abrupt meteorological changes or possible

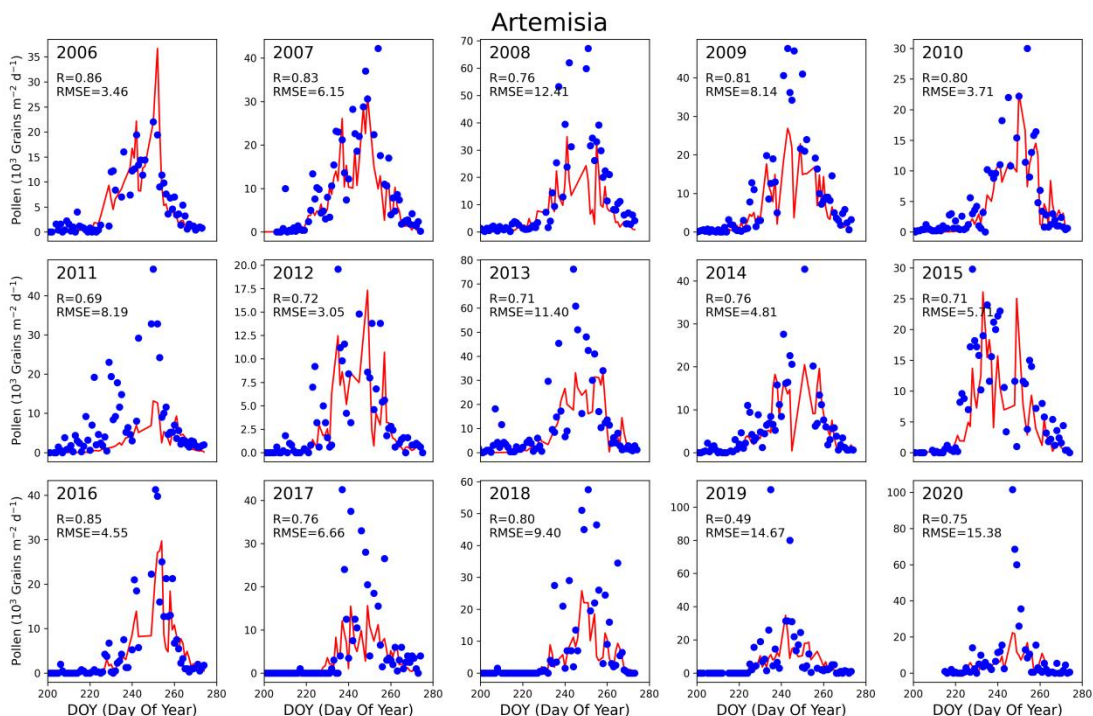
708 issues with the quality of observation data. The RegCM accurately simulates the
709 sDOY and eDOY, displaying a similar frequency to observations. For peak pollen
710 simulations, years such as 2006, 2007, 2010, 2012, 2015, and 2016 show good
711 performance, with R above 0.7, particularly in 2006 and 2016, where R exceeds 0.85
712 and RMSE is only 4×10^3 Grains $m^{-2} d^{-1}$. However, for other years, peak simulations
713 are underestimated to varying degrees. For 2011, although the trend is consistent, the
714 observed peak is near 50×10^3 Grains $m^{-2} d^{-1}$, while the simulated peak is only 12×10^3
715 Grains $m^{-2} d^{-1}$, indicating a significant underestimation. This underestimation is also
716 noticeable in 2008, 2013, and 2017-2020. In 2019, although the peak concentrations
717 align, the trend correlation is low (R=0.49), and RMSE is high. The variability in
718 observation station data quality and quantity could influence these results, with some
719 years having fewer than six effective stations (minimum of two), impacting the
720 average and peak values. Box plots (Fig. 11) reveal that Artemisia concentrations in
721 2019-2020 are more dispersed, suggesting possible anomalies in observation data.
722 Overall, the R for RegCM simulations ranges from 0.69 to 0.86 (except 2019), with
723 RMSE between $3.05-15.38 \times 10^3$ Grains $m^{-2} d^{-1}$.

724 For Chenopod simulations (Fig. S11), the overall performance is similar to
725 Artemisia. The annual peak concentrations are generally lower, around $20-50 \times 10^3$
726 Grains $m^{-2} d^{-1}$, except for 2007, which reaches 120×10^3 Grains $m^{-2} d^{-1}$. The years
727 2006, 2008-2009, 2012-2013, 2015, and 2019 show good simulation performance,
728 accurately reflecting peak concentrations, particularly in 2016 (R=0.84,
729 RMSE= 3.11×10^3 Grains $m^{-2} d^{-1}$). However, 2007, 2010, 2017-2018, and 2020 exhibit
730 underestimation, with the exceptionally high observed concentrations in 2007 likely
731 causing the model's underestimation. Fig. 11 indicates increasing peak concentrations
732 in recent years (2017-2020) for both Artemisia and Chenopod, with room for
733 improvement in peak simulations by the RegCM. Despite the lower concentrations
734 compared to spring pollen, autumn pollen significantly impacts pollen-induced
735 diseases (pollinosis), prompting more attention and efforts in pollen management,
736 which contributes to the decreasing trend in monitored pollen concentrations.

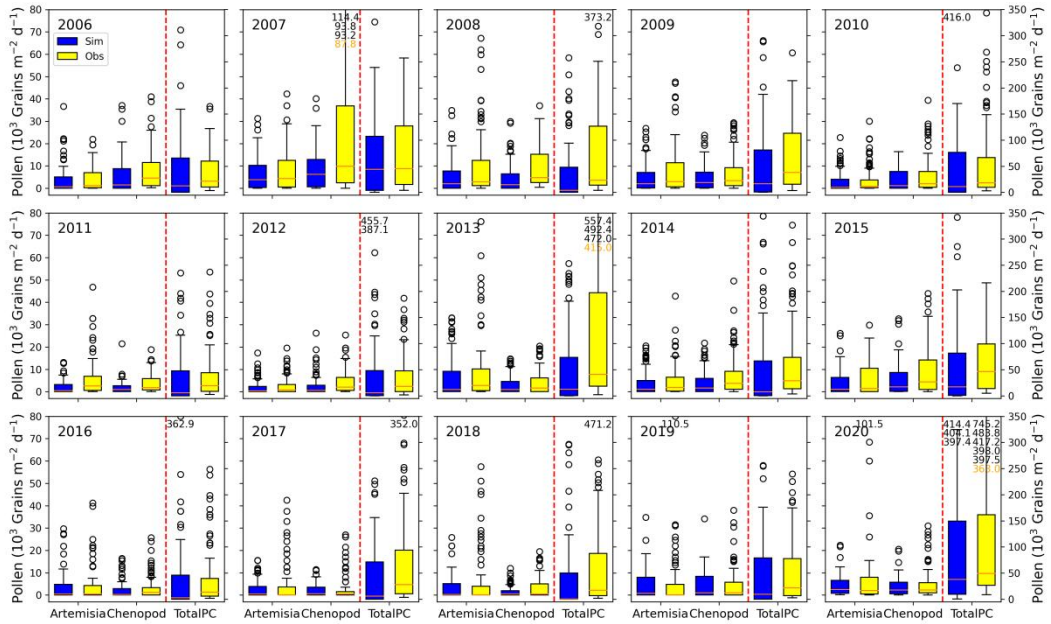
737 TotalPC generally exhibits higher concentration levels compared to Artemisia

738 and Chenopod (Fig. S12). Annual peak TotalPC can reach $150\text{--}500 \times 10^3$ Grains $\text{m}^{-2} \text{d}^{-1}$,
 739 with the highest observed concentration in 2020 at 745×10^3 Grains $\text{m}^{-2} \text{d}^{-1}$. Due to the
 740 higher quality and completeness of TotalPC monitoring data, the simulation results
 741 are more accurate, with R generally above 0.76 (except 2015, $R=0.64$). Over 60 % of
 742 the years have R above 0.8, with fewer years showing significant underestimation of
 743 peak concentrations (e.g., 2013). This highlights the critical role of high-quality
 744 pollen monitoring data for accurate simulations. High-quality data enable precise
 745 capturing of pollen concentration trends and peaks, providing robust support for
 746 regional pollen phenology research.

747 In summary, the RegCM demonstrates high accuracy in simulating the
 748 concentrations of the three pollen types, especially TotalPC. Accurate simulations of
 749 pollen concentrations and peaks enhance the effectiveness of pollen emissions models,
 750 improve health risk warnings, and provide a scientific basis for urban planning and
 751 environmental management.



752
 753 Fig. 10. Time-series distribution of Artemisia under RegCM simulation compared to observations
 754 (averaged across effective pollen monitoring sites). The red solid line represents model
 755 simulations, while blue dots depict observations



756

757 Fig. 11. Box plot statistics of pollen concentration under RegCM simulation compared to observed
 758 values. Each subplot features box plots denoted by red dashed lines: on the left side, representing
 759 Artemesia and Chenopod concentrations with values referenced on the left y-axis; on the right side,
 760 depicting TotalPC with values referenced on the right y-axis. In each box plot, from bottom to top,
 761 the box and whiskers indicate the minimum, lower quartile, median, upper quartile, and maximum
 762 values (extending up to 1.5 times the interquartile range, IQR). Black circles denote outliers
 763 exceeding 1.5 times IQR. Orange numbers annotated in the subplot indicate the maximum values
 764 unseen within the box, while black numbers denote unseen outliers

765

4. Conclusion

766 This study utilized years of autumn pollen concentration data from Beijing,
 767 alongside meteorological and land use data, to develop an autumn pollen emissions
 768 model using autumn phenology and the RF algorithm. We conducted an in-depth
 769 analysis of the spatiotemporal distribution characteristics of Artemesia, Chenopod, and
 770 TotalPC in Beijing and examined their relationships with meteorological factors.
 771 Finally, we validated the accuracy and reliability of the constructed pollen emissions
 772 model using the RegCM. Through a series of simulations and validations, several
 773 significant conclusions and findings were obtained.

774

(1) Construction of the Pollen Emissions Model: By incorporating phenology

775 and the RF algorithm, we calculated autumn pollen emissions, thereby avoiding the
776 poor simulation results of sDOY, eDOY, and annual pollen production based solely on
777 temperature linear simulations. The study demonstrates that using a phenology model
778 for sDOY and eDOY simulations captures the temporal variations of pollen release
779 more accurately, effectively reducing simulation errors. The RF algorithm excels in
780 handling multivariate and nonlinear relationships, significantly improving the
781 simulation accuracy of the pollen emissions model. The optimized annual pollen
782 production simulations better reflect seasonal changes in pollen, showcasing the
783 applicability and reliability of the RF algorithm in processing meteorological and
784 environmental data.

785 (2) Spatiotemporal Distribution Characteristics of Pollen Concentration: The
786 study found significant spatial and temporal variations in pollen concentration in
787 Beijing. The autumn pollen peak occurs between DOY 215-280, with considerable
788 differences in peak times and concentrations among monitoring stations. These
789 differences are closely related to the vegetation types, topographical features, and
790 local climatic conditions around each station. Optimized simulations of pollen
791 concentration data further reveal the spatiotemporal variation patterns of pollen
792 concentrations.

793 (3) Impact of Meteorological Factors on Annual Pollen Emissions:
794 Meteorological factors significantly influence pollen concentrations. The study
795 reveals that temperature, RH, and SSH are crucial factors affecting annual pollen
796 emissions in Beijing. There is a positive correlation between temperature and RH with
797 annual pollen emissions, while SSH has a negative correlation. The response of
798 different pollen types to meteorological factors varies due to their distinct biological
799 characteristics and ecological environments. This comprehensive analysis provides a
800 scientific basis for predicting future changes in pollen concentrations.

801 (4) Validation of Pollen Emissions Models Using the RegCM: The RegCM
802 accurately reflects the daily impact of meteorological factors on pollen emissions.
803 Key physical processes, such as advection, convection, and wet and dry deposition,
804 play essential roles in simulating the atmospheric dispersion and deposition of pollen.

805 This study validated the accuracy and reliability of the optimized emission potential
806 models for three pollen types using RegCM, effectively describing the daily variations
807 in pollen concentrations influenced by meteorological factors and key physical
808 processes. Furthermore, the pollen emissions model developed in this study can be
809 applied to other regions, offering potential for wider application. These
810 comprehensive results provide essential scientific support for pollen monitoring,
811 allergy prevention, and the selection of urban greening plants. Future research can
812 extend these methods and findings to larger-scale pollen emissions simulations and
813 forecasts, enhancing responses to pollen-related public health issues.

814 (5) Limitations and Future Prospects: Despite significant progress in
815 constructing the pollen emissions model and analyzing the spatiotemporal distribution
816 of pollen concentrations, some limitations persist. For broader application, more
817 extensive observation stations are needed to verify the model's accuracy, considering
818 the limited spatiotemporal resolution of current pollen concentration data. Simulating
819 specific species' pollen concentrations requires detailed plant functional type
820 distributions, which significantly impact the spatial distribution of pollen emissions
821 potential. The current research utilizes static plant functional type data, but dynamic
822 data would better reflect the impact of land use changes on pollen climates over
823 various temporal and spatial scales. Additionally, the complex relationship between
824 meteorological factors and pollen concentrations suggests that future research could
825 introduce more environmental and meteorological variables and apply advanced
826 machine learning algorithms to enhance the model's predictive capability.

827 In conclusion, This study successfully constructed a pollen emissions potential
828 model, systematically analyzed the spatiotemporal distribution of different pollen
829 types in autumn in Beijing, and explored their relationship with meteorological factors.
830 The model's accuracy and stability were validated using the RegCM, yielding notable
831 research results. Future research can further validate and extend this approach on a
832 larger scale and with higher resolution, providing comprehensive scientific support
833 for ecological environment protection and public health.

834 **Data availability**

835 Meteorological data were sourced from the China Surface Climate Daily Dataset
836 (<https://data.cma.cn/data/cdcindex/cid/f0fb4b55508804ca.html>), which requires
837 appropriate permissions for access. Pollen data were provided by the Beijing
838 Meteorological Bureau, and the authors do not have permission to share this data.

839 **Authorship contributions**

840 **JL** performed the analysis, investigation, methodology, software development,
841 validation, and original draft preparation. **XA** conceptualized the paper, provided
842 resources, acquired funding, and conducted the review and editing. **ZS** and **CY**
843 contributed resources, visualization, and data curation. **HQ**, **YZ**, and **ZL** were
844 involved in visualization. All authors contributed to manuscript revisions.

845 **Declaration of competing interest**

846 The authors declare that they have no known competing financial interests or personal
847 relationships that could have appeared to influence the work reported in this paper.

848 **Acknowledgments**

849 This work was supported by the National Key Research and Development
850 Program of China (grant number 2022YFC3701205), Science and Technology
851 Development Fund of the Chinese Academy of Meteorological Sciences (grant
852 number 2023Z026) and the National Natural Science Foundation of China (grant
853 number 41975173).

854 **Reference**

855 Aerts, R., M. Stas, N. Vanlessen, M. Hendrickx, N. Bruffaerts, L. Hoebelke, N. Dendoncker, S.
856 Dujardin, N. D. Saenen & A. Van Nieuwenhuyse (2020) Residential green space and seasonal
857 distress in a cohort of tree pollen allergy patients. International Journal of Hygiene and
858 Environmental Health, 223, 71-79.
859 Ahmed, A., A. Hakim & A. Becker (2018) Evaluation of eczema, asthma, allergic rhinitis and

860 allergies among the Grade-1 children of Iqaluit. *Allergy Asthma Clin. Immunol.* 14, 9.

861 Asher, M.I., S. Montefort, B. Björkstén, C.K. Lai, D.P. Strachan, S.K. Weiland & H. Williams
862 (2006) Worldwide time trends in the prevalence of symptoms of asthma, allergic
863 rhinoconjunctivitis, and eczema in childhood: ISAAC Phases One and Three repeat
864 multicountry cross-sectional surveys. *Lancet* 368, 733–743.

865 Bai, Y., X. Liu, M. Sun, G. Liu & Y. Meng (2009) Effect of Pollen Pollution on Human Health.
866 *Journal of Anhui Agri. Sci.*, 37(5), 2220-2222. (in Chinese)

867 Bastl, K., M. Kmenta, M. Berger & U. Berger (2018) The connection of pollen concentrations and
868 crowd-sourced symptom data: new insights from daily and seasonal symptom load index data
869 from 2013 to 2017 in Vienna. *World Allergy Organization Journal*, 11, 1-8.

870 Bishan, C., L. Bing, C. Chixin, S. Junxia, Z. Shulin, L. Cailang, Y. Siqiao & L. Chuanxiu (2020)
871 Relationship between airborne pollen assemblages and major meteorological parameters in
872 Zhanjiang, South China. *PLOS ONE*, 15, e0240160.

873 Breiman, L. (2001) Random Forests. *Machine Learning*, 45, 5-32.

874 Chen, H., J. Li, L. Cheng, Z. Gao, X. Lin, R. Zhu, L. Yang, A. Tao, H. Hong & W. Tang (2021)
875 China consensus document on allergy diagnostics. *Allergy, Asthma & Immunology Research*,
876 13, 177.

877 Chen, J., S. Zhu, P. Wang, Z. Zheng, S. Shi, X. Li, C. Xu, K. Yu, R. Chen, H. Kan, H. Zhang & X.
878 Meng (2024) Predicting particulate matter, nitrogen dioxide, and ozone across Great Britain
879 with high spatiotemporal resolution based on random forest models. *Science of The Total
880 Environment*, 926, 171831.

881 Cingi, C., P. Gevaert, R. Møsge, C. Rondon, V. Hox, M. Rudenko, N.B. Muluk, G. Scadding, F.
882 Manole, C. Hupin, W.J. Fokkens, C. Akdis, C. Bachert, P. Demoly, J. Mullol, A. Muraro, N.
883 Papadopoulos, R. Pawankar, P. Rombaux, E. Toskala, L. Kalogjera, E. Prokopakis, P.W.
884 Hellings & J. Bousquet (2017) Multimorbidities of allergic rhinitis in adults: European
885 academy of allergy and clinical immunology task force report. *Clin. Transl. Allergy* 7, 17.

886 D'Amato, G., C. Vitale, M. Lanza, A. Molino & M. D'Amato (2016) Climate change, air pollution,
887 and allergic respiratory diseases: an update. *Current opinion in allergy and clinical
888 immunology*, 16, 434-440.

889 Damialis, A., C. Fotiou, J. M. Halley & D. Vokou (2011) Effects of environmental factors on

890 pollen production in anemophilous woody species. *Trees*, 25, 253-264.

891 Emanuel, M.B. (1988) Hay fever, a post industrial revolution epidemic: a history of its growth
892 during the 19th century. *Clin. Allergy* 18, 295–304.

893 Frei, T. & E. Gassner (2008) Climate change and its impact on birch pollen quantities and the start
894 of the pollen season an example from Switzerland for the period 1969–2006. *International*
895 *Journal of Biometeorology*, 52, 667-674.

896 Gao, Q.Q., Q.Y. Gao, J. Li, F. Shen, S. Ji & L. Guan (2022) Preliminary Study on the Variation
897 Characteristics of Pollen Concentration and Pollen Allergy Grade in Langfang Area in Spring.
898 *Journal of Agricultural Catastrophology*. 12(10): 16-18.(in Chinese)

899 Gu, D. & K. Liao (2003) The relationship between urban pollen dispersal and meteorological
900 conditions. *Hubei Meteorology*, (03): 36-37. (in Chinese)

901 Guan, L., Q.Y. Gao, H. Li, J. Li & Q.Q. Gao (2021) Characteristics of Airborne Pollen Variation in
902 Langfang City and Its Relationship with Meteorological Factors. *Agricultural technology*
903 *service*. 38(6):93-98.(in Chinese)

904 Guzman, A., L. Tonelli, D. Roberts, J. Stiller, M. Jackson, J. Soriano, S. Yousufi, K. Rohan, H.
905 Komarow & T. Postolache. 2007. Mood-worsening with high-pollen-counts and seasonality:
906 a preliminary report. In *Journal of affective disorders*.

907 He, H., D. Zhang & B. Qiao (2001) Preliminary approach of the relationship between Airborne
908 pollen amount and meteorological factors in Beijing urban area. *Chin J Microbiol Immunol*.
909 (S2):36-38. (in Chinese)

910 He, X., D. Liu, Y. Pan, X. He, M. Zhang & S. Yang (2023) Distribution and sources of fluvial
911 pollen in the middle reaches of the Yellow River in China and their relationship with
912 vegetation and land use. *Science of The Total Environment*, 856, 159109.

913 Helbig, N., B. Vogel, H. Vogel, and F. Fiedler, 2004: Numerical modelling of pollen dispersion on
914 the regional scale. *Aerobiologia*, 20, 3-19.

915 Ibrahim, N.M., F.I. Almarzouqi, F.A. Al Melaih, H. Farouk, M. Alsayed & F.M. AlJassim (2021)
916 Prevalence of asthma and allergies among children in the United Arab Emirates: a
917 cross-sectional study. *World Allergy Organ. J.* 14, 100588.

918 Khwarahm, N. R., J. Dash, C. A. Skjøth, R. M. Newnham, B. Adams-Groom, K. Head, E. Caulton
919 & P. M. Atkinson (2017) Mapping the birch and grass pollen seasons in the UK using satellite

920 sensor time-series. *Science of The Total Environment*, 578, 586-600.

921 Krishna, M. T., P. A. Mahesh, P. K. Vedanthan, V. Mehta, S. Moitra & D. J. Christopher (2020)

922 The burden of allergic diseases in the Indian subcontinent: barriers and challenges. *The*

923 *Lancet Global Health*, 8, e478-e479.

924 Kurganskiy, A., S. Creer, N. De Vere, G. W. Griffith, N. J. Osborne, B. W. Wheeler, R. N. McInnes,

925 Y. Clewlow, A. Barber & G. L. Brennan (2021) Predicting the severity of the grass pollen

926 season and the effect of climate change in Northwest Europe. *Science Advances*, 7,

927 eabd7658.

928 Lake, I. R., N. R. Jones, M. Agnew, C. M. Goodess, F. Giorgi, L. Hamaoui-Laguel, M. A.

929 Semenov, F. Solomon, J. Storkey & R. Vautard (2017a) Climate change and future pollen

930 allergy in Europe. *Environmental health perspectives*, 125, 385-391.

931 Lei, Y., Y. Miao, Y. Zhao, S. Zhang, H. Cao, X. Lan, Z. Zhang & H. Jin (2023) The effects of

932 meteorological conditions on allergenic airborne pollen in arid Northwest China.

933 *Atmospheric Environment*, 299, 119647.

934 Li, L., D. Hao, X. Li, M. Chen, Y. Zhou, D. Jurgens, G. Asrar & A. Sapkota (2022) Satellite-based

935 phenology products and in-situ pollen dynamics: A comparative assessment. *Environmental*

936 *Research*, 204, 111937.

937 Li, X., Y. Zhou, L. Meng, G. Asrar, A. Sapkota & F. Coates (2019) Characterizing the relationship

938 between satellite phenology and pollen season: A case study of birch. *Remote Sensing of*

939 *Environment*, 222, 267-274.

940 Li, Z., Y. Chen, Y. Tao, X. Zhao, D. Wang, T. Wei, Y. Hou & X. Xu (2023) Mapping the personal

941 PM2.5 exposure of China's population using random forest. *Science of The Total*

942 *Environment*, 871, 162090.

943 Lou, H., S. Ma, Y. Zhao, F. Cao, F. He, Z. Liu, J. Bousquet, C. Wang, L. Zhang & C. Bachert

944 (2017) Sensitization patterns and minimum screening panels for aeroallergens in

945 self-reported allergic rhinitis in China. *Scientific reports*, 7, 9286.

946 Mallol, J., J. Crane, E. von Mutius, J. Odhiambo, U. Keil & A. Stewart (2013) The international

947 study of asthma and allergies in childhood (ISAAC) phase three: a global synthesis. *Allergol.*

948 *Immunopathol.* 41, 73-85.

949 Meier, M. & C. Bigler (2023) Process-oriented models of autumn leaf phenology: ways to sound

950 calibration and implications of uncertain projections. *Geosci. Model Dev.*, 16, 7171-7201.

951 Meng, L., X. Wang, Z. Ouyang, Y. Ren & Q. Wang (2016) Seasonal Dynamics of Airborne Pollens
952 and Its Relationship with Meteorological Factors in Beijing Urban Area. *Environmental
953 science*. 37 (02): 452-458.(in Chinese)

954 Mir, E., C. Panjabi & A. Shah (2012) Impact of allergic rhinitis in school going children. *Asia
955 Pacific Allergy*, 2, 93-100.

956 Mo, Y., J. Zhang, H. Jiang & Y. H. Fu (2023) A comparative study of 17 phenological models to
957 predict the start of the growing season. *Frontiers in Forests and Global Change*, 5.

958 National Cooperative Group on Childhood Asthma, 1993. A nationwide survey on the prevalence
959 of asthma among 0-14 year old population in China(1988~1990). *Chin. J. Tuberc. Respir. Dis.*
960 16, 64–68. <https://doi.org/10.3760/cma.j.issn.1001-0939.1993.Z1.143>.

961 National Cooperative Group on Childhood Asthma, 2003. A nationwide survey in China on
962 prevalence of asthma in urban children. *Chin. J. Pediatr.* 41, 123–127. <https://doi.org/10.3760/cma.j.issn.0578-1310.2003.02.116>.

963 National Cooperative Group on Childhood Asthma, Institute of Environmental Health and Related
964 Product Safety, Chinese Center for Disease Control and Prevention, Chinese Center for
965 Disease Control and Prevention, 2013. Third nationwide survey of childhood asthma in urban
966 areas of China. *Chin. J. Pediatr.* 51, 729–735.

967 Oleson, K., D. Lawrence, G. Bonan, M. Flanner & E. Kluzeck (2010) Technical Description of
968 Version 4.0 of the Community Land Model (CLM), NCAR Technical Note
969 NCAR/TN-478+STR, NCAR, Boulder, USA, 257 pp.

970 Qiao, Y., L. Wu, S. Yang, Q. Wang, H. Gu, L. Wei, G. Liu, S. Zhou, P. Wang & M. Song (2023)
971 Metabolomic and transcriptomic analyses provide insights into variations in flavonoids
972 contents between two *Artemisia* cultivars. *BMC Plant Biology*, 23, 288.

973 Rahman, A., C. Luo, B. Chen, S. Haberle, M. H. R. Khan, W. Jiang, R. Xiang, J. Liu, L. Wang, G.
974 Lin, M. Yang & V. Thilakanayaka (2020) Regional and seasonal variation of airborne pollen
975 and spores among the cities of South China. *Acta Ecologica Sinica*, 40, 283-295.

976 Schmidt, C.W. (2016) Pollen overload: seasonal allergies in a changing climate. *Environ. Health
977 Perspect.* 124.

978 Septembre-Malaterre, A., M. Lalarizo Rakoto, C. Marodon, Y. Bedoui, J. Nakab, E. Simon, L.

980 Hoarau, S. Savriama, D. Strasberg, P. Guiraud, J. Selambarom & P. Gasque (2020) *Artemisia*
981 *annua*, a Traditional Plant Brought to Light. *International Journal of Molecular Sciences*, 21.

982 Sofiev, M., P. Siljamo, H. Ranta & A. Rantio-Lehtimäki (2006) Towards numerical forecasting of
983 long-range air transport of birch pollen: theoretical considerations and a feasibility study.
984 *International Journal of Biometeorology*, 50, 392-402.

985 Sofiev, M., P. Siljamo, H. Ranta, T. Linkosalo, S. Jaeger, A. Rasmussen, A. Rantio-Lehtimaki, E.
986 Severova & J. Kukkonen (2013) A numerical model of birch pollen emissions and dispersion
987 in the atmosphere. Description of the emission module. *International Journal of*
988 *Biometeorology*, 57, 45-58.

989 Stas, M., R. Aerts, M. Hendrickx, A. Delcloo, N. Dendoncker, S. Dujardin, C. Linard, T. Nawrot,
990 A. Van Nieuwenhuyse & J.-M. Aerts (2021) Exposure to green space and pollen allergy
991 symptom severity: A case-crossover study in Belgium. *Science of The Total Environment*,
992 781, 146682.

993 Valipour Shokouhi, B., K. de Hoogh, R. Gehrig & M. Eeftens (2024) Estimation of historical daily
994 airborne pollen concentrations across Switzerland using a spatio temporal random forest
995 model. *Science of The Total Environment*, 906, 167286.

996 Virro, H., A. Kmoch, M. Vainu & E. Uuemaa (2022) Random forest-based modeling of stream
997 nutrients at national level in a data-scarce region. *Science of The Total Environment*, 840,
998 156613.

999 Wang, X. D., M. Zheng, H. Lou, C. Wang, Y. Zhang, M. Bo, S. Ge, N. Zhang, L. Zhang & C.
1000 Bachert (2016) An increased prevalence of self-reported allergic rhinitis in major Chinese
1001 cities from 2005 to 2011. *Allergy*, 71, 1170-1180.

1002 Wang, X. Y., T. T. Ma, X. Y. Wang, Y. Zhuang, X. D. Wang, H. Y. Ning, H. Y. Shi, R. L. Yu, D.
1003 Yan & H. D. Huang (2018) Prevalence of pollen-induced allergic rhinitis with high pollen
1004 exposure in grasslands of northern China. *Allergy*, 73, 1232-1243.

1005 Wozniak, M. C. & A. L. Steiner (2017) A prognostic pollen emissions model for climate models
1006 (PECM1.0). *Geosci. Model Dev.*, 10, 4105-4127.

1007 Wu, Z., A. Liu, Y. Bai, B. Liu & C. Wang (2011) Study on Evaluation of Economic Benefits from
1008 Pollen Forecast and Service in Tianjin. *Meteorological monthly*. 37(5):626-632.(in Chinese)

1009 Yin, J., F. Yue, L. Wang, H. He, T. Xu, H. Zhang, H. Li, L. Wen, J. Sun & J. Gu (2005) The

1010 clinical study of the relationship between allergic rhinitis and allergic asthma in the patients
1011 with autumnal pollinosis. *Zhonghua Yi Xue Za Zhi*, 85, 1683-1687.

1012 Yorimitsu, Y., A. Kadosono, Y. Hatakeyama, T. Yabiku & O. Ueno (2019) Transition from C3 to
1013 proto-Kranz to C3-C4 intermediate type in the genus *Chenopodium* (Chenopodiaceae).
1014 *Journal of Plant Research*, 132, 839-855.

1015 Zhang, Y. & A. L. Steiner (2022) Projected climate-driven changes in pollen emissions season
1016 length and magnitude over the continental United States. *Nature Communications*, 13, 1234.

1017 Zhao, Y., Z. Sun, L. Xiang, X. An, X. Hou, J. Shang, L. Han & C. Ye (2023) Effects of pollen
1018 concentration on allergic rhinitis in children: A retrospective study from Beijing, a Chinese
1019 megacity. *Environmental Research*, 229, 115903.